From large-amplitude kinetic Alfvén fluctuations to kinetic turbulence at proton scales

C. L. Vásconez[1], F. Valentini[2], O. Pezzi[2], S. Servidio[2], F. Malara[2], F. Pucci[3]

[1] *Departamento de Física, Escuela Politécnica Nacional, Quito, Ecuador*

[2] *Dipartimento di Fisica, Università della Calabria, Rende (Cs), Italia*

[3] *Center for Mathematical Plasma Astrophysics, Universiteit Leuven, Leuven, Belgium*

Abstract

Turbulence in the solar wind has been extensively studied, both by detailed analyses of in situ measurements and from a theoretical point of view [1]. Beside the homogeneous turbulence, generation of small scale fluctuations can take place also in other realistic configurations. Recent numerical simulations of these kind of configurations have shown that phase mixing of large-scale parallel-propagating Alfvén waves is an efficient mechanism for the production of kinetic Alfvén waves at wavelengths close to d_p and at a large propagation angle with respect to the magnetic field [2]. Many observational [3] and theoretical works [4] have suggested that these fluctuations may play a determinant role in the development of the solar-wind turbulent cascade. In this work, we study numerically large amplitude KAW fluctuations in inhomogeneous backgrounds and their effects on the protons by means of hybrid Vlasov-Maxwell simulations [5]. For this, the kinetic dynamics of protons has been investigated by varying both the magnetic configuration and the amplitude of the initial perturbations. Of interest here is the transition from quasi-linear to turbulent regimes, focusing, in particular, on the development of important non-Maxwellian features in the proton distribution function driven by KAW fluctuations.

Introduction

Beside the homogeneous turbulence, generation of small scale fluctuations takes place also in more realistic configurations, for instance, an Alfvén wave propagating in a medium where the Alfvén velocity varies in a direction transverse to $\mathbf{B}_0$ undergoes phase-mixing [6], which progressively bends wavefronts thus generating small scales in the transverse direction. As suggested by [2, 7] the dynamics of Alfvén waves with shears can be crucial for the understanding of more realistic scenarios, such as the turbulent solar wind, the magnetosheet and the inhomogeneous regions of the solar corona. Hence the key-point is now to understand the transition from KAWs to turbulence.

Setup of the hybrid Vlasov-Maxwell simulations

Together with the choice of an isothermal equation of state for the electrons, of constant pressure P_e, we can write the dimensionless hybrid Vlasov-Maxwell (HVM) equations [5]:

$$\frac{\partial f}{\partial t} + \mathbf{v}\cdot\nabla f + (\mathbf{E} + \mathbf{v}\times\mathbf{B})\cdot\frac{\partial f}{\partial \mathbf{v}} = 0; \quad \mathbf{E} = -(\mathbf{u}\times\mathbf{B}) + \frac{1}{n}(\mathbf{j}\times\mathbf{B} - \nabla P_e); \tag{1}$$

$$\frac{\partial \mathbf{B}}{\partial t} = -\nabla\times\mathbf{E}; \quad \nabla\times\mathbf{B} = \mathbf{j}, \tag{2}$$

where f is the proton distribution function, $\mathbf{j}$ is the current density, $\mathbf{u}$ is the bulk velocity, $\mathbf{E}$ and $\mathbf{B}$ are the electric and magnetic fields, respectively; the displacement current has been neglected in the Ampere equation, and quasi-neutrality is assumed. These normalized HVM equations has been solved in a 2D-3V phase-space configuration. The spatial domain has been chosen double periodic, $D = L\times L = [0, 16\pi]\times[0, 16\pi]$. Meanwhile, in the three-dimensional velocity box, $f = 0$ for $|v| > vmax = 5v_{thp}$, in each velocity direction. This velocity space is discretized with $N_{V_x} = N_{V_y} = N_{V_z} = 51$ grid points, while in the physical space we employed $N_x = 256$ grid points in the x direction, and $N_y = 1024$ grid points in the y direction. We choose, for the equilibrium magnetic field $B^{(0)}(y)$, a nearly homogeneous field both in the central part (b_M), and in the two lateral regions of the domain (b_m) (see Figure 1). Two runs were performed, with different values for b_M and b_m (see Table 1). In both runs the jump in the magnetic-field magnitude through the shear regions is the same, while in RUN I larger values of b_M and b_m have been used, respect to RUN II. Equilibrium values for the total pressure $P_T^{(0)}$ and for the temperature $T^{(0)}$ are also in Table 1.

Table 1: Simulations setup.

RUN	b_M	b_m	$T^{(0)}$	$P_T^{(0)}$	a
I	1.5	1	0.5	1.748	0.2
II	0.8	0.3	0.125	0.4	0.3

At time $t = 0$, an Alfvénic perturbation of amplitude a is imposed on the above equilibrium. From the values of Table 1, we expect that nonlinear effects are more relevant in RUN II than in RUN I, showing a transition to turbulence.

In Figure 1, the profiles of the Alfvén velocity associated to the equilibrium structure (left panel), and the proton beta $\beta_p^{(0)}$ (right panel) are plotted for RUN I (black curve), and for RUN II (red curve). Here, we can easily identify the shear layers and the homogeneity regions.

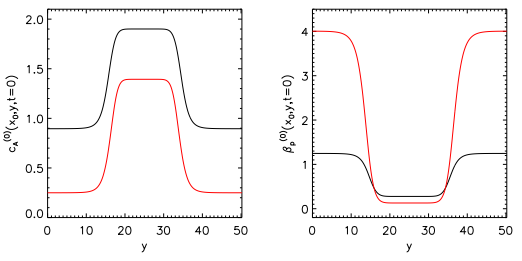

Figure 1: *Profiles of $c_A^{(0)}(y)$ (left panel) and $\beta_p^{(0)}(y)$ (right panel) for RUN I (black curve) and RUN II (red curve).*

Results

To characterize and compare the two runs, we have computed the measure of deviation of the proton VDF from the Maxwellian to the configuration shape, $\varepsilon(x,y,t)$ [8]. Figure 2 shows the time evolution of $\varepsilon_{max}(t) = \max_D\{\varepsilon(x,y,t)\}$ (the maximum value of ε over the domain D). We can see that the saturation level of ε_{max} increases as the initial perturbation amplitude increases. This tell us that where the nonlinear effects are more relevant (RUN II), the kinetic processes work more efficiently to drive the protons away from the thermodynamic equilibrium. The vertical blue-dashed line corresponds to the theoretical estimation of t^*, at which phase-mixing produces transverse scales of the order of the proton inertial length d_p.

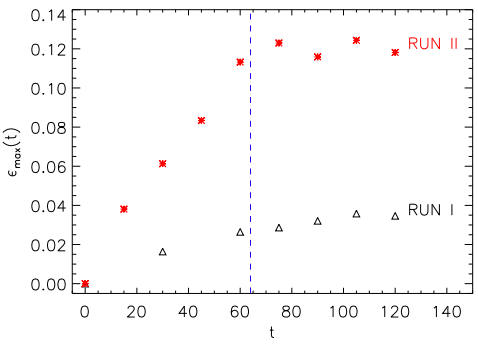

Figure 2: *Time evolution of ε_{max} computed from the VDFs of RUN I (black triangles) and RUN II (red stars).*

In Figure 3, the contour plots of $|\mathbf{j}|$ (left column), ε (middle column), and $\delta T = T - T^{(0)}$ (right column) are presented for RUN I (upper row), and for RUN II (lower row). These contour plots are obtained for the time $t = t^* = 105$. Going from RUN I to RUN II, $|\mathbf{j}|$, originally concentrated near the shear regions [panel (a)], becomes more intense and tends to filament when kinetic physics gets dominant [panel (d)].

Non-Maxwellian features in RUN I are essentially located within the shear regions, near the peaks of $|\mathbf{j}|$ (panel (b)). In RUN II, such features are still peaked in the shear regions where dispersive effects responsible for the KAW formation are active. However, significant departures from Maxwellianity are visible also in the lateral homogeneous regions, starting from the early stage of the simulation (not shown). Finally, also temperature variations exhibit a behavior similar to that of ε, being more intense in the shear regions for RUN I as compared to RUN II, in which significant values of δT are recovered in the whole spatial domain.

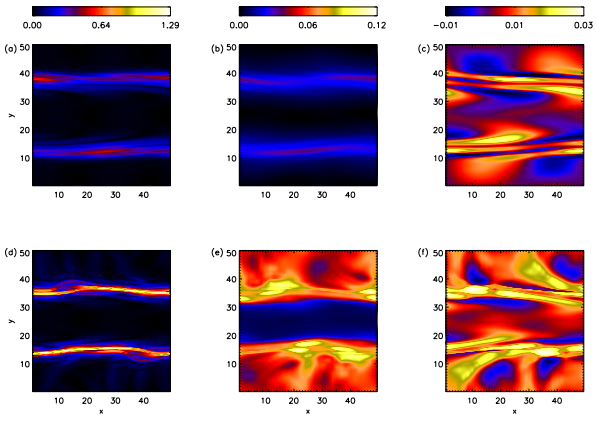

Figure 3: *2D contour plots, at $t = 105$, of $|\mathbf{j}|$ (left column), ε (middle column), and δT (right column), for RUN I (upper row) and RUN II (bottom row).*

Three-dimensional surface plots of the proton VDF at t^* are presented in Figure 4. Computed at the spatial point where $\varepsilon = \varepsilon_{max}$ for each run. The unit vector of the local magnetic field is displayed in these plots as a magenta tube. In the left plot (RUN I), one notices smooth deviations of the particle VDF from the spherical Maxwellian shape, with the appearance of a barely visible bulge along the local field and a ring-like modulation in the perpendicular plane. Here, the direction of the local field seems to be still a preferred direction of symmetry for the particle VDF. On the other hand, for RUN III (right plot), when the transition to a turbulent state has been observed, any symmetry is lost, as sharp gradients and small-scale velocity structures have been produced through the nonlinear interaction of protons with the turbulent fields [9].

Summary and Conclusions

As recently shown by [2, 7], KAWs are naturally generated through the phase-mixing mechanism, when Alfvén waves propagate in an inhomogeneous medium. In the present paper, we reproduced numerically, through 2D-3V Hybrid Vlasov-Maxwell simulations, the generation of KAWs by imposing Alfvénic perturbations on an initial pressure balanced magnetic shear equilibrium. Both the characteristic of the initial equilibrium and the amplitude of the perturbations have been varied, in order to explore the system dynamics in different regimes, focusing, in particular, on the transition from a linear to a turbulent regime. Moreover, as the HVM code provides an almost noise-free description of the proton distribution function, we have shown how the interaction of large amplitude KAW fluctuations with protons shapes the VDF and make it depart from local thermodynamic equilibrium.

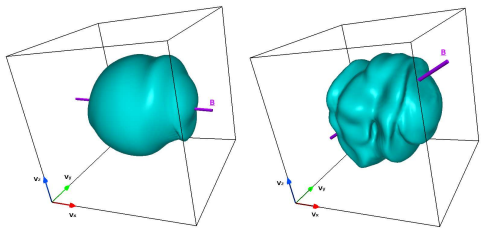

Figure 4: *Iso-surface plots of the proton VDF in velocity space, at the spatial location where ε is maximum for RUN I (left) and RUN II (right); the magenta tubes indicate the direction of the local magnetic field.*

References

[1] Bruno, R. & Carbone, V. 2005, Living Reviews in Solar Physics, 2, 4

[2] Vásconez, C. L., Pucci, F., Valentini, F., et al. 2015, ApJ, 815, 7

[3] Kiyani, K. H., Chapman, S. C., Sahraoui, F., et al. 2013, ApJ, 763, 10

[4] Sahraoui, F., Belmont, G., & Goldstein, M. 2012, ApJ, 748, 100

[5] Valentini, F., Trávníček, P., Califano, F., Hellinger, P., & Mangeney, A. 2007, JCP, 225, 753

[6] Heyvaerts, J. & Priest, E. 1983, A & A, 117, 220

[7] Pucci, F., Vásconez, C. L., Pezzi, O., et al. 2016, JGR: Space Physics, 121, 1024

[8] Greco, A., Valentini, F., Servidio, S., & Matthaeus, W. 2012, Physical Review E, 86, 066405

[9] Valentini, F., Vásconez, C.L., Pezzi, O., Servidio, S., Malara, F.,Pucci, F. 2017, A&A, 599, A8